Deterministic conversion between memory and threshold resistive switching via tuning the strong electron correlation

Peng, Haiyang; Li, Yongfeng; Lin, Wei Nan; Wang, Yu Zhan; Gao, Xing Yu; Wu, Tom

2012

Peng, H. Y., Li, Y. F., Lin, W. N., Wang, Y. Z., Gao, X. Y., & Wu, T. (2012). Deterministic conversion between memory and threshold resistive switching via tuning the strong electron correlation. Scientific Reports, 2(442).

https://hdl.handle.net/10356/96101

https://doi.org/10.1038/srep00442

SCIENTIFIC REPORTS

OPEN

SUBJECT AREAS:
MATERIALS PHYSICS
ELECTRONIC MATERIALS AND DEVICES
MODELLING AND THEORY
MATERIALS SCIENCE

Received
30 November 2011

Accepted
30 April 2012

Published
7 June 2012

Correspondence and requests for materials should be addressed to T.W. (tomwu@ntu.edu.sg)

Deterministic conversion between memory and threshold resistive switching via tuning the strong electron correlation

Hai Yang Peng[1], Yong Feng Li[1], Wei Nan Lin[1], Yu Zhan Wang[2], Xing Yu Gao[2,3] & Tom Wu[1]

[1]Division of Physics and Applied Physics, School of Physical and Mathematical Sciences, Nanyang Technological University, 637371 Singapore, [2]Physics Department, National University of Singapore, 2 Science Drive 3, 117542 Singapore, [3]Shanghai Institute of Applied Physics, Chinese Academy of Sciences, 239 Zhang Heng Road, Pudong New District, Shanghai, 201203 P. R. China.

Intensive investigations have been launched worldwide on the resistive switching (RS) phenomena in transition metal oxides due to both fascinating science and potential applications in next generation nonvolatile resistive random access memory (RRAM) devices. It is noteworthy that most of these oxides are strongly correlated electron systems, and their electronic properties are critically affected by the electron-electron interactions. Here, using NiO as an example, we show that rationally adjusting the stoichiometry and the associated defect characteristics enables controlled room temperature conversions between two distinct RS modes, i.e., nonvolatile memory switching and volatile threshold switching, within a single device. Moreover, from first-principles calculations and x-ray absorption spectroscopy studies, we found that the strong electron correlations and the exchange interactions between Ni and O orbitals play deterministic roles in the RS operations.

It has been known for decades that the strong correlation between electrons in complex oxides gives rise to rich physics such as high temperature superconductivity, colossal magnetoresistance, multiferroics, and so on[1–3]. In a seemingly parallel line of research, nonlinear electronic transport phenomena in transition metal oxides, in particular electrical-field-induced reversible resistive switching (RS), have also attracted lots of attention[4–9]. The recent fast advances on resistive switching have been driven by the relentless quests for the next-generation nonvolatile resistive random access memory (RRAM) devices[10–13]. The resistive switching phenomenon has been reported in a wide variety of materials, including binary oxides[14–18], perovskite[19–21], chalcogenides[22–24], and even organic materials[25–26]. Although the common metal-insulator-metal capacitor-like structure of RRAM is deceptively simple, the physical mechanisms remain elusive, and different mechanisms based on thermochemical and electrochemical effects have been invoked to explain the rich phenomena[27].

According to the volatility, there are two primary types of RS: Nonvolatile memory switching in which both the low resistance state (LRS) and high resistance state (HRS) can be retained even after the external voltage is removed, and threshold switching in which only the HRS is stable at low bias voltages[28]. It is of key technological importance to understand exactly the conditions triggering the onset of memory and threshold RS as well as the underlying mechanisms. If unintentionally incorporated into nonvolatile memory cells, threshold switching can be detrimental to the reliable operation of integrated circuits as a result of its volatile nature. On the other hand, controllably realizing both memory and threshold switching in the same device can bring along technological benefits: While the former is the key to realize the nonvolatile information storage, the later can serve as a selector in series with a memory cell to solve the sneak path problem in cross-point or multistack structures[29–30]. This scheme possesses advantages over the conventional approaches where transistors or diodes are used as cell selectors in terms of integration density and simple processing. However, the difference between memory and threshold RS is quite subtle, and it remains a challenge for individual memory devices to controllably toggle between the two modes.

Notably, many RRAM materials are strongly correlated electron systems, e.g., NiO is a prototypical Mott insulator which is predicted to be a metal by the conventional band theory, but is an insulator instead as a result of the strong Coulomb repulsion between electrons[31–33]. RS in NiO was first reported in the 1960s[34], and mechanisms involving thermochemical formation and rupture of conducting filaments are often invoked to account for the unipolar switching in NiO[27]. In transition metal oxides, it is well known that the strong electron correlation can

split the energy bands, affecting electronic band structures and transport properties. Furthermore, the correlation effect can be tailored via tuning various factors like sample stoichiometry, strain and external fields, rendering lots of flexibility in rational material designs. Since resistive switching is an electronic (ionic) phenomenon by nature, the many-body mutual interactions among electrons should play important roles. Indeed, it was recently proposed that Mott insulator-to-metal transition is responsible for the nonvolatile resistive switching in some ternary chalcogenides[35–36]. However, in general, it is not clear how the strong correlation between electrons influences the switching characteristics in RRAM devices.

Here we show that the volatility of resistive switching can be reliably tuned by adjusting the defect characteristics, electronic correlation, and the corresponding band structure in NiO. We demonstrate deterministic conversions between the nonvolatile memory switching and the threshold switching at room temperature within individual devices. Rationally adjusting the device configuration (i.e., bottom electrode) and measurement protocols (i.e., compliance current) can dynamically tune the stoichiometry and defect characteristics, enabling the conversions between different switching modes. Our first-principles calculations and x-ray absorption spectroscopy studies further confirm that the strong correlations and exchange between electron orbitals play key roles in the operation of RS devices made of transition metal oxides.

Results

We illustrate the key idea in **Figure 1**. As shown in **Figure 1a**, NiO is a charge-transfer insulator, whose band gap is between the oxygen 2*p* band and the nickel 3*d* upper Hubbard band[31]. The intra-atomic *d*-*d* Coulomb energy U is a direct result of the strong electron correlation. Since the first ionization state is of primarily oxygen 2*p* character rather than of nickel 3*d* character, the charge-fluctuation energy is determined by the change transfer gap (Δ) $d^8 \rightarrow d^9\underline{L}$, where $\underline{L}$ denotes a hole in the oxygen valence band. This charge transfer process is analogous to the redox reaction, involving electron transfer between oxygen and nickel, which is believed to play the pivotal role in memory switching[27]. As a charge-transfer insulator, NiO exhibits the voltage-controlled memory RS behavior (**Fig. 1b**). On the other hand, tuning the chemical stoichiometry in NiO can effectively modify the electron correlation and cause the band splitting. As shown in **Figure 1c**, the nickel deficiency decreases the charge transfer gap Δ and changes NiO toward the negative-charge-transfer insulator type[31], in which the band gap is not of the *p*-to-*d* nor *d*-to-*d* but *p*-*p* type, $d^8\underline{L} + d^8\underline{L} \leftrightarrow d^8 + d^8\underline{L}^2$, with a considerable mixture of *d* character into the *p* states. Our key hypothesis is that this alteration of the band structure will drastically affect the switching and give rise to the voltage-controlled threshold switching in RS devices made of Ni-deficient NiO (**Fig. 1d**).

Experimentally, NiO thin films with a thickness of 200 nm were grown using pulsed laser deposition (PLD), and they exhibit good crystalline quality (see Supplementary Fig. S1 online). We found that selecting the bottom electrode and adjusting the switching conditions are effective to tune the volatility of resistive switching, which, as we will show later, is linked with the modifications of stoichiometry in NiO. In polycrystalline NiO thin films prepared on tin-doped indium oxide (ITO) coated glass substrates, we observed the typical unipolar memory switching when a compliance current (CC) of 1 mA was used in the set operation **(Fig. 2a)**. This memory switching in the NiO/ITO device is stable and reproducible with good endurance and retention (see Supplementary Fig. S2 online). The threshold switching was obtained when the CC was increased to 10 mA, which corresponds to a current density of 44.4 A/cm^2 (**Fig. 2b**). Even after the CC returned back to 1 mA, the threshold switching persisted, as shown in **Figure 2c**. On the other hand, the reference NiO devices fabricated on a Pt layer (200 nm) coated Si wafer show only memory switching as the CC varies between 1 and 10 mA (see Supplementary Fig. S1 online). This contrast underscores the critical role of the bottom electrode.

In RS, the existence and migration of oxygen vacancies often play important roles[27], and the extended defects can even lead to the

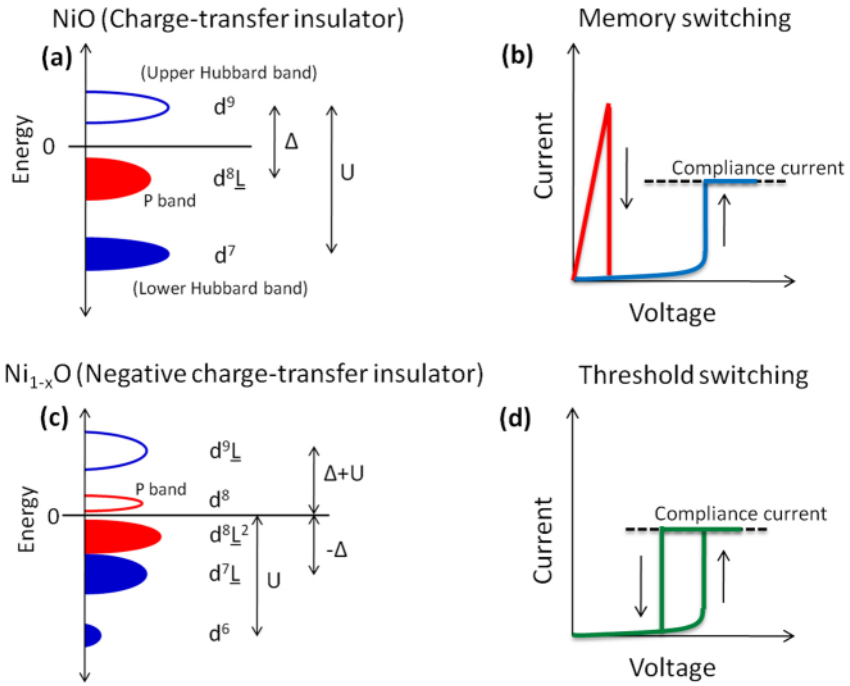

Figure 1 | Schematics illustrating the correlation between the band structure and the RS volatility. (a) Energy diagram of NiO as a charge-transfer insulator. Δ denotes the energy of the ligand-to-metal charge-transfer, $d^8 \rightarrow d^9\underline{L}$ ($\underline{L}$: ligand hole). U represents the intra-atomic *d*-*d* Coulomb energy. Correspondingly, we observed (b) voltage-controlled memory switching. (c) Energy diagram of non-stoichiometric $Ni_{1-x}O$ which can be classified as a negative-charge-transfer insulator, where the band gap is determined by the split oxygen 2*p* bands. In devices made of such Ni-deficient NiO, we observed (d) voltage-controlled threshold switching.

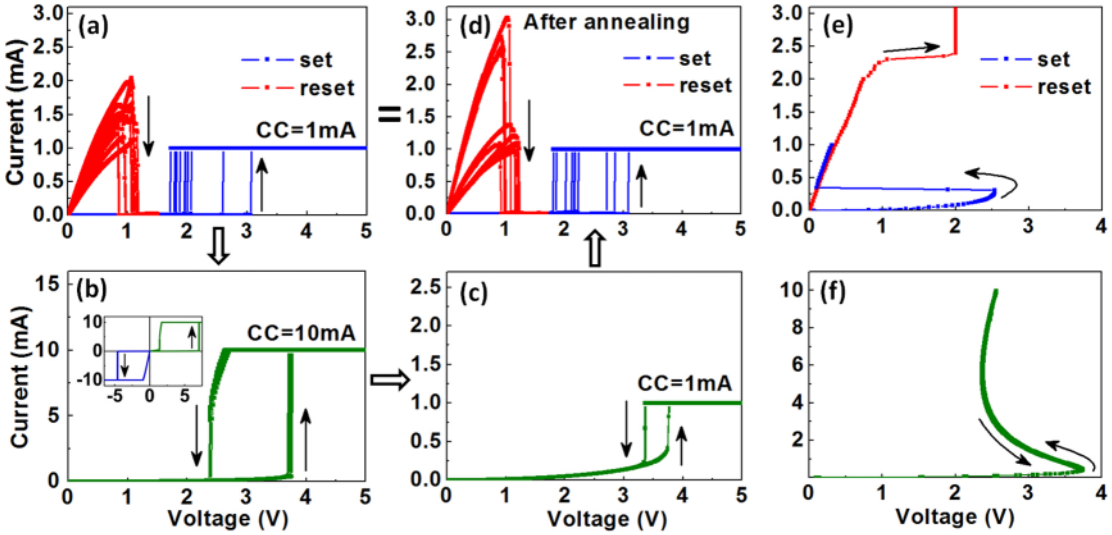

Figure 2 | Conversions between memory and threshold switching modes. (a) Memory switching was observed in the Pt/NiO/ITO device when a compliance current (CC) of 1 mA was used. The blue and red lines represent ten set and reset cycles, respectively. (b) Threshold switching was achieved when CC was increased to 10 mA. Ten cycles of operation are shown. Inset: Polarity dependence of the forming process, and only the positive bias leads to the threshold switching. (c) Threshold switching was retained even after CC was reduced to 1 mA, while the hysteresis loop became smaller. (d) After annealing in vacuum at 300°C for 30 minutes, the threshold switching was converted back to the memory switching which resembles the data shown in (a). (e) Current-controlled memory switching. A compliance voltage of 2 V was used during the reset operation. (f) Current-controlled sweeping curve corresponding to the voltage-controlled threshold switching mode, exhibiting negative differential resistance.

formation of nanoscale Ni-rich metallic filaments[37]. Thus, it is reasonable to speculate that the type of volatility may be related to the film stoichiometry, in particular the oxygen content. To verify this hypothesis, we annealed the device showing the threshold switching (Fig. 2c) in vacuum (0.01 Pa) at 300°C for 30 minutes. Interestingly, the threshold switching was converted back to the memory switching, as shown in **Figure 2d**. If we increase the CC to 10 mA, we can achieve the memory switching again. This indicates that, compared to annealing in vacuum, increasing CC produces the opposite effect, presumably via modulating the film stoichiometry.

The memory and the threshold switching modes correspond to different current-controlled sweeping behaviors. As shown in **Figure 2e**, the Pt/NiO/ITO device showed expected memory switching in the current-controlled mode. In this case, voltage was monitored and a compliance voltage of 2 V was used during the reset process. On the other hand, when the device is characterized with the threshold switching (Fig. 2b), no sharp resistive switching was observed under the current controlled mode (**Fig. 2f**). Instead, a smooth current controlled negative differential resistance (CC-NDR) was observed within the voltage range from 2.4 to 3.7 V, which is exactly equal to the two threshold voltages in the voltage controlled mode (Fig. 2b). Although the voltage controlled threshold switching and CC-NDR are often reported separately[4–5,28], here we show that they can manifest in the same device.

To further analyze the stoichiometry of devices showing different switching behaviors, we performed the time-of-flight secondary ion mass spectroscopy (TOF-SIMS) measurements after the devices were switched to different states and compared the data to the standard NiO sample. The SIMS profiles of normalized O/Ni ratios for different switching states are shown in **Figure 3a**. In general, the O/Ni ratio is higher near the interface of NiO/ITO because the ITO bottom electrode serves as a reservoir of oxygen ions. All depth-resolved compositional profiles exhibit notable fluctuations; nevertheless, in average, the O/Ni ratio is the highest in the threshold OFF state, and the lowest in the memory ON state. This is consistent with the previous reports where the threshold switching was observed in Ni-deficient NiO films[14]. Since in NiO the formation energies of vacancies are much lower than those of interstitials[38], the off-stoichiometry in different switching states can be attributed to the presence of either oxygen or nickel vacancies. The estimated average concentrations of oxygen vacancies in the memory OFF and ON state are 6.3 at.% and 7.7 at.%, respectively; this off-stoichiometry could be related to the existence of Ni-rich metallic nanofilaments which were suggested to be essential for RS in NiO[37]. On the other hand, the average concentration of nickel vacancies in the threshold OFF state is approximately 1.5 at.%.

The enhanced O/Ni ratio in the threshold OFF state as compared to the pristine state has implications on the conduction mechanisms. The *I-V* curves of both states follow the Poole-Frenkel (PF) mechanism[30]. The PF effect describes the high-electric-field-assisted conduction in insulators, which can be quantitatively expressed as follows:

$$In(J/E) \propto q\left(\sqrt{\frac{qE}{\pi\varepsilon_0\varepsilon_i}} - \phi_B\right) \Big/ kT \qquad (1)$$

where, J is the current density, E is the applied electrical field, q is the electronic charge, ε_0 is the permittivity of free space, ε_i is the dielectric constant, ϕ_B is the barrier height, k is the Boltzmann constant, and T is the temperature. As shown in **Figure 3b**, both the *I-V* curves of the pristine state and the threshold OFF state can be well simulated by the PF conduction model. The dielectric constants (ε_i) extracted from our fitting are 10.9 and 11.9 for the pristine state and the threshold OFF state, respectively. As a higher ε implies a higher oxygen concentration[30,39–40], our data confirm that the threshold OFF state has more oxygen than the pristine state. We also directly prepared NiO samples under different oxygen pressures, and indeed the high pressure grown sample shows the threshold switching while the lower pressure grown sample shows the memory switching (see Supplementary Fig. S3 online). As shown in **Figure 3c**, these variations of composition in different RS states affect the dynamic diffusion of oxygen ions, and as we will discuss later, the modified rupture and formation of conducting filaments lead to different types of RS volatility.

To elucidate the relationship between the nickel deficiency and the electronic band structure, we performed first-principles calculations

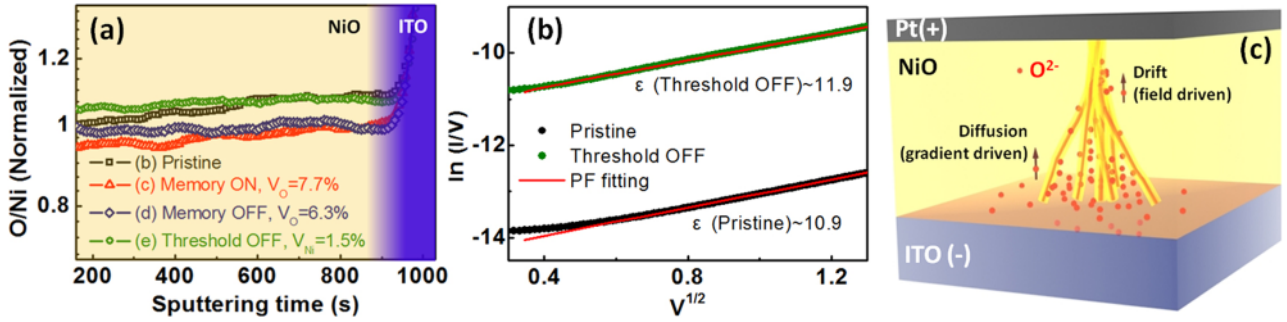

Figure 3 | Determination of compositions in various RS states. (a) SIMS profiles for different RS states. In comparison to the stoichiometric pristine state, the estimated average concentrations of oxygen vacancies are 7.7% and 6.3% for the memory ON and OFF states, respectively. The average concentration of nickel vacancies is 1.5% for the threshold OFF state. (b) PF emission fittings to the pristine and the threshold OFF states. The derived dielectric constant of the threshold OFF state is larger than that of pristine state, in line with the SIMS result that the O/Ni ratio is higher in the threshold OFF state. (c) Schematic of the Ni-rich metallic filament in NiO whose formation and rupture is the result of dynamic competition between the oxygen-gradient-induced drift and the field-induced diffusion motions of the oxygen ions.

on NiO with different chemical stoichiometry. A supercell of $Ni_{32}O_{32}$ (2×2×2 unit cells) was used. **Figure 4a and 4b** show the density of states (DOS) for ideal $Ni_{32}O_{32}$ and Ni-deficient $Ni_{31}O_{32}$, respectively. As expected, the electronic band structure of $Ni_{32}O_{32}$ represents a typical charge-transfer insulator, where the valence band showing primarily the oxygen 2*p* character and the conduction band mainly the nickel 3*d* character[41–42]. In contrast, for the supercell of $Ni_{31}O_{32}$ containing one nickel vacancy, the charge transfer energy Δ becomes smaller and turns even negative. The Fermi level enters the oxygen 2*p* band and the Coulomb repulsion causes the band splitting, in a way analogous to some formally Ni^{3+} oxides[31]. In this sense, NiO with nickel vacancies is a negative-charge-transfer insulator, in which both of the conduction band maximum and the valence band minimum are primarily of the oxygen 2*p* band character. Although other defects besides Ni vacancy and their complexes may exist in NiO, the calculation here captures the basic physics regarding the band structure of Ni-deficient NiO, and more sophisticated models can be developed in the future to shed light on the various physical states during RS operations.

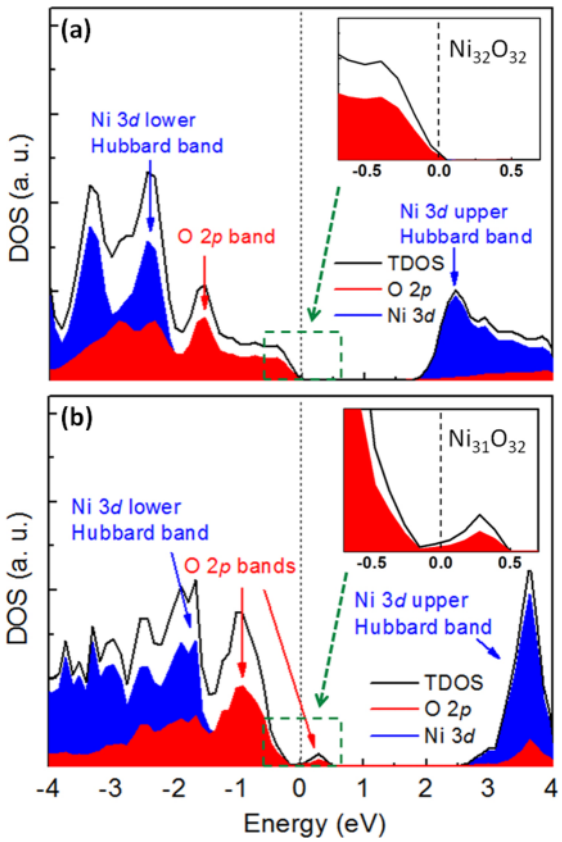

Figure 4 | Calculated band structures of stoichiometric and Ni-deficient NiO. (a) Calculated density of states (DOS) of NiO. A supercell of $Ni_{32}O_{32}$ was used. In additional to the total DOS (black lines), partial contributions from O 2*p* and Ni 3*d* are also shown. Inset is the enlarged view of the region near the Fermi level. The band gap is determined by the ligand-to-metal charge-transfer energy. (b) Calculated DOS of Ni-deficient NiO as simulated by $Ni_{31}O_{32}$. Inset is the enlarged view of the DOS near the Fermi level. As a result of the Ni deficiency, the oxygen-derived band expands across the Fermi level and splits due to the Coulomb repulsion between electrons. In this case, the band gap is determined by the negative-charge-transfer gap.

To confirm the theoretical result that the Ni-deficient NiO is a negative-charge-transfer insulator, we performed the x-ray absorption spectroscopy (XAS) measurements on NiO samples prepared at two different oxygen pressures. Our compositional analysis indicated that the growth pressure is effective in tuning the stoichiometry of the NiO films; an oxygen pressure of 0.01 Pa results in the stoichiometric composition, while various degrees of Ni deficiency was detected in samples grown at high oxygen pressures. As shown in **Figure 5**, for both samples, peak B at 530.5 eV in the O K-edge spectra corresponds to the transition from the O 1*s* level to the states with O 2*p*

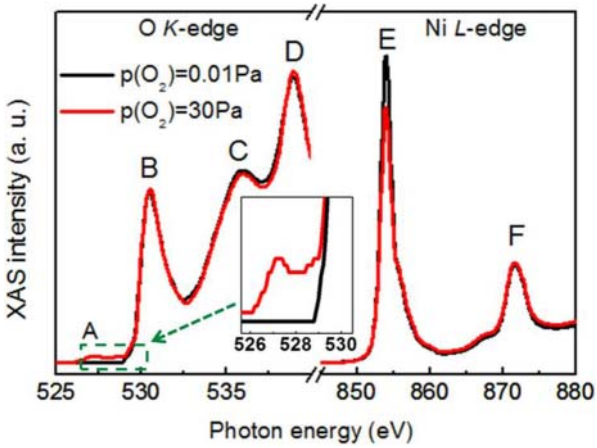

Figure 5 | X-ray absorption spectra of NiO. Oxygen *K*-edge (left) and Ni *L*-edge (right) XAS spectra for NiO prepared in different oxygen ambient, namely 0.01 Pa (black line) and 30 Pa (red line). The inset highlights the onset of peak A in the sample grown at the higher oxygen pressure.

character in the upper Hubbard band[43]. The peaks C and D can be assigned to the Ni 4*p* bands[44]. Notably, for the Ni-deficient NiO film grown at the higher oxygen pressure, a new peak A centered at 527.3 eV was observed (inset of Fig. 5), which can be attributed to the transition from O 1*s* to the nickel vacancies induced O 2*p* states right above the Fermi level[44–45]. This is consistent with the calculated result that this high-pressure NiO sample is a negative-charge-transfer insulator. At the Ni *L*-edge, the peaks E and F can be assigned to Ni $2p_{3/2}$ and Ni $2p_{1/2}$ to Ni 3*d* transitions, respectively[46]. In addition, the absence of any shift in peaks E and F at the Ni *L*-edge suggests that the nickel-deficiency-induced holes have more O 2*p* character than Ni 3*d* character[43,47], which is consistent with the result of our first-principles calculations (**Fig. 4b**).

Discussion

The experimental results outlined above suggest a coherent mechanism governing the physical properties and the switching characteristics in NiO. Factors including the selection of the bottom electrode, adjusting the CC, and the annealing treatments can effectively modulate the defect chemistry, giving rise to different switching volatilities. In the conventional thin film synthesis and device operation, the compositions of the films are often assumed to be fixed by the experimental conditions used in the synthesis. However, as we have shown here, the spatial distribution of defects and the associated stoichiometry can be dynamically tuned during the operation of the RS devices. Furthermore, the profiles of composition and temperature can be very inhomogeneous and percolative in nature, and it is demanding to understand the complex kinetics.

In a simplified picture, during RS operations, the oxygen distribution and the related dynamics can be described by a general 1-D ionic model[48–50], involving O^{2-} ions hopping between potential wells. In the Pt/NiO/ITO device, the concentration of O^{2-} ions (C) is both time and location dependent (**Fig. 3c**). As confirmed in the SIMS data (**Fig. 3a**), ITO bottom electrode can be taken as a reservoir of oxygen ions, and the gradient of oxygen ions is the driving force behind their diffusion. In this process, the diffusion coefficient is given by:

$$D = D_0 \cdot \exp(-E_a/kT), \tag{2}$$

where D_0 is a constant determined by the attempt-to-escape frequency and the effective hopping distance, and E_a is the activation energy of the oxygen vacancy diffusion. In addition, an applied electric field can cause a drift motion of O^{2-} ions with an average velocity υ. Taking both the electrical drift and the thermal diffusion into consideration, we get the continuity equation which describes the dynamic evolution of the oxygen concentration C:

$$\frac{\partial C}{\partial t} = D\frac{\partial^2 C}{\partial x^2} + \upsilon\frac{\partial C}{\partial x} - \frac{C}{\tau}, \tag{3}$$

where τ is the lifetime associated with the recombination rate of oxygen ions with species like metallic nickel and oxygen vacancies. On the right hand side of Equation (3), the first and second terms elucidate the competition between the thermal diffusion and the electrical drift of the oxygen ions, which dictates the localized formation and dissolution of the conducting filaments in NiO during switching.

In the Pt/NiO/ITO device, the applied electrical field causes the drift of the oxygen ions, facilitating the local reduction of NiO and the formation of metallic conducting filaments. On the other hand, when a higher CC is used, e.g., 10 mA in **Figure 2b**, a substantial Joule heating is generated, which promotes the diffusion of oxygen ions from ITO into NiO as the diffusion coefficient in Equation (2) increases with temperature. This diffusion process not only eliminates the oxygen vacancies, but also introduces nickel vacancies in NiO, presumably resulting in weaker conducting filaments as well as the observed threshold switching (**Fig. 2c**). Furthermore, the Joule heating weakens the fragile conducting filaments, and the ruptures lead to the threshold switching[51]. This scenario of migrating oxygen ions is also consistent with the observation that the transition from memory to threshold switching was only observed when the Pt top electrode was positively biased (inset of **Fig. 2b**). When a negative bias is applied to the top Pt electrode, the electric field prevents the diffusion of oxygen ions from ITO, leading to the memory switching. This polarity dependence implies that the switching transition hinges on the delicately balanced migration of oxygen ions, which must be carefully considered to achieve reliable device operations.

The modification of band structure bears significance to the volatility of resistive switching. In stoichiometric NiO, a high electric field can facilitate transferring electrons from the valence band (primarily oxygen 2*p* character) into the conduction band (primarily nickel 3*d* character). This charge transfer process is analogous to the redox reaction[27,52], and the resulting metallic Ni is responsible for the formation of conducting filaments in the memory switching of NiO. On the other hand, in NiO with nickel vacancies, which is a negative-charge-transfer insulator, such a redox reaction is more difficult as the Fermi level is between the lower and the higher oxygen 2*p* bands. A low electric field mainly excite charge fluctuations between two oxygen 2*p* bands, and a stable metallic filament cannot be maintained, giving rise to the threshold switching.

In summary, with the prototypical Mott insulator NiO as an example, we shed light on the characteristics of resistive switching from the perspective of strong electron correlation effects. It is not surprising that the strong correlation between electrons can not only give rise to the complex band structures, but also affect the various aspects of transport properties including the RS phenomena. The electron correlation and the associated band structure can be modified by tailoring the device structure, the synthesis conditions, and the measurement protocols. Specifically, stoichiometric NiO is a charge-transfer insulator, where the charge fluctuation is the *p-d* type, giving rise to the commonly reported memory switching. On the other hand, the oxygen-rich ITO bottom electrode and the high CC lead to the enhanced diffusion of oxygen ions, facilitating the conversion from the memory to the threshold switching. Our first-principles calculations and XAS measurements suggest that the nickel-deficient nickel oxide, namely $Ni_{1-x}O$, is a negative-charge-transfer insulator, where the charge fluctuation is mainly the *p-p* type. Among the various factors considered so far in literature, the strong correlation effect between electrons has been largely ignored in interpreting resistive switching experiments. Our study suggests that the strong electron correlation effect does profoundly affect the characteristics of resistive switching, and its general role in the operation of memory devices made of transition metal oxides clearly warrants further investigations.

Methods

Thin films deposition and characterization. NiO thin films were fabricated on ITO-coated glass substrates or Pt-coated Si wafers at 450°C using pulsed laser deposition (PLD) with a solid state Nd:YAG laser ($\lambda = 532$ nm). The structural characterization was carried out by using high-resolution x-ray diffraction (XRD). Using the cross-sectional SEM, we estimated the thickness of the NiO films to be about 200 nm.

Device fabrication and measurement. Pt top electrodes with a typical area of 150 μm × 150 μm were deposited on the NiO thin films by sputtering through a shadow mask at room temperature, and post annealed at 200°C in air to improve the contact quality. The *I-V* curves of the RRAM devices were obtained using a Keithley 4200 Semiconductor Characterization System. To prevent permanent dielectric breakdown, compliance current (CC) was implemented during all measurements.

SIMS analysis and XAS measurement. In the depth-resolved SIMS elemental analysis, a larger top electrode size of 500 μm × 500 μm was used to make sure that the sputtered area during the SIMS measurements is within the electrodes. The XAS measurements were carried out at the SINS beamline (SINS) of the Singapore Synchrotron Light Source. The spectra were measured in the total electron yield (TEY) mode with the p-polarized light, and the photon energy resolution E/ΔE was set at about 1000.

First-principles calculations. The spin-polarized DOS calculations were carried out using the frozen-core projector-augmented wave (PAW) method[53–54] within the frame of density functional theory (DFT) as implemented in the VASP codes[55–56]. The generalized gradient approximation (GGA) for electron exchange and correlation were performed[53,57]. Furthermore, on-site Coulomb repulsion U was taken into account as a result of the strong correlation effect of Ni 3d states at the Hartree Fock level ($U = 6.3$ eV and $J = 1$ eV)[38]. The cutoff energy for the plane-wave basis set was 400 eV. A rock-salt structural NiO supercell with 64 atoms was employed, and for the Ni vacancy calculation a Ni atom was removed from the supercell. All the atoms were allowed to relax until the Hellmann-Feynman forces become less than 0.01 eV/Å. The calculated lattice constant of the perfect NiO is 4.17 Å, which is in good agreement with the experimental value[58].

1. Dagotto, E. Correlated electrons in high-temperature superconductors. *Rev. Mod. Phys.* **66**, 763–840 (1994).
2. Imada, M., Fujimori, A. & Tokura, Y. Metal-insulator transitions. *Rev. Mod. Phys.* **70**, 1039–1263 (1998).
3. Salamon, M. B. & Jaime, M. The physics of manganites: Structure and transport. *Rev. Mod. Phys.* **73**, 583–628 (2001).
4. Hickmott, T. W. Low-frequency negative resistance in thin anodic oxide films. *J. Appl. Phys.* **33**, 2669–2682 (1962).
5. Simmons, J. G. & Verderbe, R. R. New conduction and reversible memory phenomena in thin insulating films. *Proc. R. Soc. London., Ser. A, Math.* **301**, 77–102 (1967).
6. Ovshinsky, S. R. Reversible electrical switching phenomena in disordered structures. *Phys. Rev. Lett.* **21**, 1450–1453 (1968).
7. Dearnale, G., Stoneham, A. M. & Morgan, D. V. Electrical phenomena in amorphous oxide films. *Rep. Prog. Phys.* **33**, 1129–1191 (1970).
8. Yang, J. J., Borghetti, J., Murphy, D., Stewart, D. R. & Williams, R. S. A family of electronically reconfiguiable nanodevices. *Adv. Mater.* **21**, 3754–3758 (2009).
9. Yang, J. J. *et al.* Diffusion of adhesion layer metals controls nanoscale memristive switching. *Adv. Mater.* **22**, 4034–4038 (2010).
10. Waser, R. & Aono, M. Nanoionics-based resistive switching memories. *Nat. Mater.* **6**, 833–840 (2007).
11. Strukov, D. B., Snider, G. S., Stewart, D. R. & Williams, R. S. The missing memristor found. *Nature* **453**, 80–83 (2008).
12. Kwon, D. H. *et al.* Atomic structure of conducting nanofilaments in TiO_2 resistive switching memory. *Nat. Nanotechnol.* **5**, 148–153 (2010).
13. Yang, J. J. *et al.* Memristive switching mechanism for metal/oxide/metal nanodevices. *Nat. Nanotechnol.* **3**, 429–433 (2008).
14. Seo, S. *et al.* Reproducible resistance switching in polycrystalline NiO films. *Appl. Phys. Lett.* **85**, 5655–5657 (2004).
15. Shima, H. *et al.* Voltage polarity dependent low-power and high-speed resistance switching in CoO resistance random access memory with Ta electrode. *Appl. Phys. Lett.* **93**, 113504 (2008).
16. Yao, J. *et al.* Resistive switching in nanogap systems on SiO_2 substrates. *Small* **5**, 2910–2915 (2009).
17. Peng, H. Y. *et al.* Electrode dependence of resistive switching in Mn-doped ZnO: filamentary vs. interfacial mechanisms. *Appl. Phys. Lett.* **96**, 192113(2010).
18. Ye, J. Y. Nanoscale resistive switching and filamentary conduction in NiO thin films. . *Appl. Phys. Lett.* **97**, 132108(2010).
19. Nian, Y. B., Strozier, J., Wu, N. J., Chen, X. & Ignatiev, A. Evidence for an oxygen diffusion model for the electric pulse induced resistance change effect in transition-metal oxides. *Phys. Rev. Lett.* **98**, 146403 (2007).
20. Szot, K., Speier, W., Bihlmayer, G. & Waser, R. Switching the electrical resistance of individual dislocations in single-crystalline $SrTiO_3$. *Nat. Mater.* **5**, 312–320 (2006).
21. Wu, S. X., Peng, H. Y. & Wu, T. Concurrent novolatile resistance and capacitance switching in $LaAlO_3$. *Appl. Phys. Lett.* **98**, 093503 (2011).
22. Henisch, H. K. Amorphous semiconductor switching. *Nature* **236**, 205–207 (1972).
23. Terabe, K., Hasegawa, T., Nakayama, T. & Aono, M. Quantized conductance atomic switch. *Nature* **433**, 47–50 (2005).
24. Schoen, D. T., Xie, C. & Cui, Y. Electrical switching and phase transformation in silver selenide nanowires. *J. Am. Chem. Soc.* **129**, 4116–4117 (2007).
25. Carchano, H., Lacoste, R. & Segui, Y. Bistable electrical switching in polymer thin films. *Appl. Phys. Lett.* **19**, 414 (1971).
26. Scott, J. C. & Bozano, L. D. Nonvolatile memory elements based on organic materials. *Adv. Mater.* **19**, 1452–1463 (2007).
27. Waser, R., Dittmann, R., Staikov, G. & Szot, K. Redox-based resistive switching memories - nanoionic mechanisms, prospects, and challenges. *Adv. Mater.* **21**, 2632–2663 (2009).
28. Chang, S. H. *et al.* Occurrence of both unipolar memory and threshold resistance switching in a NiO film. *Phys. Rev. Lett.* **102**, 026801 (2009).
29. Lee, M. J. *et al.* Two series oxide resistors applicable to high speed and high density nonvolatile memory. *Adv. Mater.* **19**, 3919–3923 (2007).
30. Hwang, I. *et al.* Resistive switching transition induced by a voltage pulse in a Pt/NiO/Pt structure. *Appl. Phys. Lett.* **97**, 052106 (2010).
31. Tsuda, N., Nasu, K., Fujimori, A. & Siratori, K. *Electronic Conduction in Oxides* (Springer, Berlin, 2000).
32. Mott, N. F. The basis of the electron theory of metals, with special reference to the transition metals. *Proc. Phys. Soc. Lond. Sect. A* **62**, 416–422 (1949).
33. Hubbard, J. Electron correlations in narrow energy bands. *Proc. R. Soc. London., Ser. A, Math.* **276**, 238–257 (1963).
34. Gibbons, J. F. & Beadle, W. E. Switching properties of thin NiO films. *Solid-State Electron.* **7**, 785–797 (1964).
35. Inoue, I. H. & Rozenberg, M. J. Taming the Mott transition for a novel Mott transistor. *Adv. Funct. Mater.* **18**, 2289–2292 (2008).
36. Cario, L., Vaju, C., Corraze, B., Guiot, V. & Janod, E. Electric-field-induced resistive switching in a family of Mott insulators: Towards a new class of RRAM Memories. *Adv. Mater.* **22**, 5193–5197 (2010).
37. Lee, M. J. *et al.* Electrical manipulation of nanofilaments in transition-metal oxides for resistance-based memory. *Nano Lett.* **9**, 1476–1481 (2009).
38. Zhang, W. B., Yu, N., Yu, W. Y. & Tang, B. Y. Stability and magnetism of vacancy in NiO: a GGA+U study. *Eur. Phys. J. B* **64**, 153–158 (2008).
39. Wu, J. B., Nan, C. W., Lin, Y. H. & Deng, Y. Giant dielectric permittivity observed in Li and Ti doped NiO. *Phys. Rev. Lett.* **89**, 217601 (2002).
40. Lin, Y. H., Wang, J. F., Jiang, L., Chen, Y. & Nan, C. W. High permittivity Li and Al doped NiO ceramics. *Appl. Phys. Lett.* **85**, 5664–5666 (2004).
41. Zaanen, J., Sawatzky, G. A. & Allen, J. W. Band-gaps and electronic-structure of transition-metal compounds. *Phys. Rev. Lett.* **55**, 418–421 (1985).
42. Fujimori, A. & Minami, F. Valence-band photoemission and optical-absorption in nickel compounds. *Phys. Rev. B* **30**, 957–971 (1984).
43. Ditusa, J. F. *et al.* Magnetic and charge dynamics in a doped one-dimensional transition-metal oxide. *Phys. Rev. Lett.* **73**, 1857–1860 (1994).
44. Soriano, L. *et al.* The electronic-structure of mesoscopic NiO particles. *Chem. Phys. Lett.* **208**, 460–464 (1993).
45. Kuiper, P., Kruizinga, G., Ghijsen, J., Sawatzky, G. A. & Verweij, H. Character of holes in $Li_xNi_{1-x}O$ and their magnetic-behavior. *Phys. Rev. Lett.* **62**, 221–224 (1989).
46. Barman, S. R., Chainani, A. & Sarma, D. D. Covalency-driven unusual metal-insulator-transition in nickelates. *Phys. Rev. B* **49**, 8475–8478 (1994).
47. Uchimoto, Y., Sawada, H. & Yao, T. Changes in electronic structure by Li ion deintercalation in $LiNiO_2$ from nickel L-edge and O K-edge XANES. *J. Power Sources* **97-98**, 326–327 (2001).
48. Mott, N. F. & Gurney, R. W. *Electronic Processes in Ionic Crystals* (Oxford University Press, Oxford, 1948).
49. Strukov, D. B. & Williams, R. S. Exponential ionic drift: fast switching and low volatility of thin-film memristors. *Appl. Phys. A-Mater. Sci. Process* **94**, 515–519 (2009).
50. Yu, S. M. & Wong, H. S. P. A phenomenological model for the reset mechanism of metal oxide RRAM. *IEEE Electron Device Lett.* **31**, 1455–1457 (2010).
51. Chang, S. H. *et al.* Effects of heat dissipation on unipolar resistance switching in Pt/NiO/Pt capacitors. *Appl. Phys. Lett.* **92**, 183507 (2008).
52. Kim, K. M., Jeong, D. S. & Hwang, C. S. Nanofilamentary resistive switching in binary oxide system: a review on the present status and outlook. *Nanotechnology* **22**, 254002 (2011).
53. Blochl, P. E. Projector augmented-wave method. *Phys. Rev. B* **50**, 17953–17979 (1994).
54. Kresse, G. & Joubert, D. From ultrasoft pseudopotentials to the projector augmented-wave method. *Phys. Rev. B* **59**, 1758–1775 (1999).
55. Kresse, G. & Hafner, J. *Ab initio* molecular-dynamics for liquid-metals. *Phys. Rev. B* **47**, 558–561 (1993).
56. Kresse, G. & Hafner, J. *Ab initio* molecular-dynamics for open-shell transition-metals. *Phys. Rev. B* **48**, 13115–13118 (1993).
57. Perdew, J. P., Burke, K. & Ernzerhof, M. Generalized gradient approximation made simple. *Phys. Rev. Lett.* **77**, 3865–3868 (1996).
58. Lide, D. R. *Handbook of Chemistry and Physics* (CRC Press, Boston, 1991).

Acknowledgments

The authors acknowledge the support from the National Research Foundation of Singapore.

Author contributions

H.Y.P. and T.W. conceived and designed the experiments. H.Y.P., W.N.L., Y. Z. Wang and X.Y.G. carried out the experiments. Y.F.L. performed the calculations. H.Y.P. and T.W. wrote the paper. All authors discussed the results and commented on the manuscript.

Additional information

Supplementary information accompanies this paper at http://www.nature.com/scientificreports

Competing financial interests: The authors declare that they have no competing financial interests.

How to cite this article: Peng, H.Y., Li, Y.F., Lin, W.N., Gao, X.Y. & Wu, T. Deterministic conversion between memory and threshold resistive switching via tuning the strong electron correlation. *Sci. Rep.* **2**, 442; DOI:10.1038/srep00442 (2012).